INTERNATIONAL JOURNAL FOR NUMERICAL METHODS IN FLUIDS
Int. J. Numer. Meth. Fluids 2006; **50**:1461–1474
Published online 9 November 2005 in Wiley InterScience (www.interscience.wiley.com). DOI: 10.1002/fld.1117

Spatial instability of a viscous liquid sheet

S. G. Chuech*,†

Department of Mechanical and Mechatronic Engineering, National Taiwan Ocean University, Keelung 20224, Taiwan

SUMMARY

In the present study, the spatial instability for a two-dimensional viscous liquid sheet, which is thinning with time, has been analysed. The study includes the derivation of a spatial dispersion equation, numerical solutions for the growth rate of sinuous disturbances, and parameter sensitivity studies. For a given wave number, the growth rate of the disturbance is essentially a function of Weber number, Reynolds number, and gas/liquid density ratio. The analysis indicates that the cut-off wave number of the disturbance becomes larger with an increase in Weber number or gas/liquid density ratio. Thus, the liquid sheet should produce finer drops. When the Reynolds number decreases, the higher viscosity has a greater damping effect on shorter waves than longer waves. This could explain that only large drops and ligaments were observed in past measurements for the disintegration of a very viscous sheet. The spatial instability results of the present study were also compared with the temporal theory. The importance of spatial analysis was found and demonstrated for the cases of low Weber numbers. The temporal theory underestimates growth rates when the Weber number is less than 100. The discrepancy between the two theories increases as the Weber number further decreases. Copyright © 2005 John Wiley & Sons, Ltd.

KEY WORDS: viscous liquid sheet; spatial instability; Newton–Raphson method

1. INTRODUCTION

The instability of a thin liquid sheet has been extensively studied for many decades because of relevance to spray nozzle performance. In the past, Squire [1] applied the temporal method of Lamb [2] to the instability analysis of sinuous disturbances on a two-dimensional inviscid liquid sheet moving in still air. Taylor [3, 4] studied the dynamics and formation of thin liquid sheets of constant thickness to understand the important phenomena of sheet breakup processes. York *et al.* [5] predicted maximum instability for the varicose wave. Haggerty and Shea [6] analysed a one-sided sheet and derived wave dispersion equations describing sinuous and varicose waves. These studies reported disturbance wave growth and the most-unstable wavelength on a sheet surface using wave dispersion equations. Their work was extended by

*Correspondence to: S. G. Chuech, Department of Mechanical and Mechatronic Engineering, National Taiwan Ocean University, Keelung 20224, Taiwan.
†E-mail: sgc@mail.ntou.edu.tw

Received 7 March 2004
Accepted 15 September 2005

others [7–9] to consider a viscous liquid film of diminishing thickness with either sinuous or varicose waves for a plane liquid sheet. Most of the studies [1–11] demonstrated that liquid sheets break up into drops through aerodynamic instability. Unstable waves can grow exponentially on the sheet surface, and then detach at the leading edge to form drops when their amplitudes are greater than a critical value. Recently, a more general type of analysis of the instability of a two-dimensional viscous liquid sheet was made by Li and Tankin [12]. Sirignano and his co-workers [13–15] investigated the linear and non-linear instability of planar liquid sheets using a vortex-dynamics model. However, most of the previous studies were limited to temporal instability analysis.

One of the serious weaknesses in the existing temporal theory for hydrodynamic instability is that disturbances are assumed to grow temporally everywhere. In reality, most fluid oscillations have amplitudes that are constant with time, but grow in a spatial direction. Gaster [16] showed that for small rates of amplification, the disturbance frequencies determined from temporal theory were approximately equal to those of the spatial analysis. He therefore concluded that the analysis should be done spatially for large amplification rates [17]. Later, several spatial studies demonstrated the important distinction for circular liquid jets [18, 19] and for liquid curtain flows [20, 21]. Since then, the spatial instability analysis for a liquid sheet has received more attention than before. Creighton and Lin [22] analysed the spatial spray formation of liquid sheets based on an energy budget. Li [23] utilized a perturbation analysis for the spatial instability study of a thin moving plane liquid sheet, and his results indicated that the spatial amplification rate depends strongly on the gas-to-liquid density ratio. Ibrahim [24] followed Levich's [25] mathematical approach to formulate the spatial dispersion equations of sinuous and varicose disturbances, and also compared his spatial growth rates with the temporal data of Li and Tankin [12]. However, all of these spatial analyses assumed that the sheet thickness is constant, and could not be applicable to most cases in reality. Although De Luca and Costa [26] developed a multiple-scale approach to obtain the spatial dispersion relations for a liquid sheet of non-uniform thickness, the role of viscosity in the evolution process of the sheet instability was eliminated with an inviscid approximation in the study.

In the present study, a spatial instability analysis was conducted for a two-dimensional viscous liquid sheet of non-constant thickness, which is a function of time. The primary goals included deriving a spatial dispersion equation, using numerical methods to solve a system of non-linear equations, comparing results with temporal analysis, and conducting a sensitivity study on critical parameters. Contrary to temporal theory, the wave number in spatial theory is complex and the wave growth rate is represented by the imaginary part of the number. The system of non-linear equations obtained from the real and imaginary parts of the spatial dispersion equation was solved simultaneously using the Newton–Raphson method. Results of the spatial instability analysis were compared with those of the temporal analysis made by Dombrowski and Johns [9]. Significant differences were found between temporal and spatial analysis for the cases of low Weber numbers. This result is similar to the spatial analysis for liquid cylindrical jets, made by Keller *et al.* [18] and Lin and Kang [19]. They found that the spatial theory predicted different results from those of temporal analysis for low-speed flow conditions.

2. GOVERNING EQUATIONS

For the present study, a viscous liquid sheet, which is thinning with time and moving in the x-direction with velocity U through stationary gas, is considered and shown in Figure 1. The

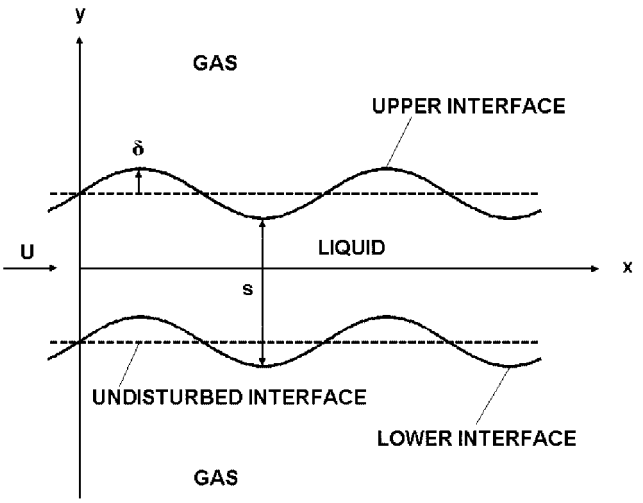

Figure 1. Sinuous disturbances of a viscous liquid sheet.

gas is assumed to be incompressible and inviscid. The linearized governing equations for the fluids subjected to sinuous perturbations in the liquid–gas interfaces are:

$$\nabla \cdot V_j = 0 \quad \text{and} \quad \rho_j \partial_t V_j = -\nabla p_j + \nabla \cdot \tau_j \tag{1}$$

where $j = 1$ denotes the gas, $j = 2$ denotes the liquid, ∂_t is the partial differential operator with respect to time t, and ∇ is a gradient operator. V is the velocity perturbation vector, p is the pressure perturbation, and τ is the shear stress. Note that the gas viscous stresses are zero in Equation (1) due to the inviscid gas assumption. For inviscid fluid flow, the velocity potential ψ satisfies the Laplace equation:

$$\nabla^2 \psi = 0 \tag{2}$$

If the velocity potential ψ is set to be equal to $\partial_t \xi$, the horizontal and vertical gas perturbation velocities can be written as

$$u_1 = \partial_t(\partial_x \xi) \quad \text{and} \quad v_1 = \partial_t(\partial_y \xi) \tag{3}$$

Thus, the gas pressure perturbation may also be obtained from the integrated momentum equation for the inviscid gas in Equation (1):

$$p_1 = -\rho_1 \partial_t^2 \xi \tag{4}$$

It is well known that there are two types of oscillations on liquid sheet surfaces, namely sinuous and varicose. The study of Dombrowski and Hooper [8] showed that the degree of varicose instability is much less than that of the sinuous mode. In other words, sinuous waves can be expected to predominate during the breakup of a film. Therefore, in the present study, only sinuous oscillation was considered for the analysis of the wave growth.

In contrast to the temporal method, both wave number and frequency in spatial theory are in a complex form (i.e. wave number $k = k_r + \mathrm{i}k_i$ and frequency $\omega = \mathrm{i}\omega_i$), where k_i represents the

spatial growth rate for a given wave number k_r and frequency ω_i. For a sinusoidal disturbance of increasing amplitude, moving along the x-axis with velocity U, the velocity potential for the inviscid gas motion can be assumed as

$$\psi = \Psi(y) \cdot e^{ik(x-Ut)+\omega t} \tag{5}$$

Substituting from Equation (5) into Equation (2) yields:

$$\partial_y^2 \Psi - k^2 \Psi = 0 \tag{6}$$

and the solution is

$$\Psi(y) = \Psi_0 \cdot e^{-ky} \tag{7}$$

Thus, the integration of Equation (5) gives

$$\xi = \frac{\Psi_0}{(\omega - ikU)} \cdot e^{k(ix-y)+(\omega-ikU)t} \tag{8}$$

For an inviscid gas, the motion of oscillations on the liquid sheet surface causes a local velocity of the gas in the y-direction, which is the vertical perturbation velocity v_1. For the boundary condition across the liquid–gas interface, the perturbation velocity should be equal to the derivative of the interface displacement δ:

$$v_1 = \partial_t \delta \tag{9}$$

Combining Equations (9) and (3), the interface displacement δ is

$$\delta = \frac{\partial \xi}{\partial y} \tag{10}$$

Furthermore, substituting from Equation (8) into Equations (4) and (10) leads to the following formulation for the gas pressure perturbation and the interface displacement:

$$p_1 = \rho_1(\omega - ikU)^2 \delta / k \tag{11}$$

and

$$\delta = \frac{-k\Psi_0}{(\omega - ikU)} \cdot e^{k(ix-y)+(\omega-ikU)t} \tag{12}$$

Considering the liquid sheet shown in Figure 1, the y-momentum equation for the liquid in Equation (1) may be integrated in the y-direction and gives

$$\rho_2 \partial_t (s \cdot \partial_t \delta) = -[(p_2)_{\text{upper}} - (p_2)_{\text{lower}}] + \mu_2 \partial_x [s \cdot \partial_x (\partial_t \delta)] \tag{13}$$

where $(p_2)_{\text{upper}}$ and $(p_2)_{\text{lower}}$ represent the liquid pressure perturbations at the upper and lower interfaces, and s is the sheet thickness. It should be noted that the thickness s is a function of time t in the present study.

In a thermodynamic equilibrium state, the free energy of a liquid–gas system has to be minimum [25]. Accordingly, for a two-dimensional system the pressure balance between two phases separated by an interface possessing surface tension σ should be

$$p_\sigma = p_1 - p_2 \tag{14}$$

where (p_σ) is the capillary pressure. Then, this relation may be applied to obtain the pressure difference between the upper and lower interfaces:

$$(p_\sigma)_{\text{upper}} - (p_\sigma)_{\text{lower}} = [(p_1)_{\text{upper}} - (p_1)_{\text{lower}}] - [(p_2)_{\text{upper}} - (p_2)_{\text{lower}}] \tag{15}$$

When a two-dimensional liquid sheet with small displacements in a thermodynamic equilibrium state is considered, the capillary pressures at the upper and lower interfaces, $(p_\sigma)_{\text{upper}}$ and $(p_\sigma)_{\text{lower}}$, are equal to $\pm\sigma\partial_x(\partial_x\delta)$, respectively [25]. Therefore, the difference between these two capillary pressures can be expressed as

$$(p_\sigma)_{\text{upper}} - (p_\sigma)_{\text{lower}} = 2\sigma \cdot \partial_x(\partial_x\delta) \tag{16}$$

Furthermore, substituting from Equations (15) and (16) into Equation (13) yields:

$$\rho_2(s \cdot \partial_t^2\delta + \partial_t s \cdot \partial_t\delta) = -[(p_1)_{\text{upper}} - (p_1)_{\text{lower}}] + 2\sigma \cdot \partial_x(\partial_x\delta) + \mu_2\partial_x[s \cdot \partial_x(\partial_t\delta)] \tag{17}$$

where $(p_1)_{\text{lower}}$ has an opposite sign to $(p_1)_{\text{upper}}$.

For simple representation and proper interpretation, all physical parameters will be normalized in a dimensionless form in the following analysis. The characteristic length in this problem is half of the sheet thickness h and the characteristic time is h/U. By substituting Equations (11) and (12) into Equation (17) and using the magnitude analysis, a dispersion equation describing the spatially growing disturbances on a two-dimensional liquid sheet can be obtained in the following dimensionless form:

$$(\Omega - \mathrm{i}K)^2 + K^2(\Omega - \mathrm{i}K)/Re + K^2/We - \rho K = 0 \tag{18}$$

where the density ratio of gas to liquid $\rho = \rho_1/\rho_2$, the Reynolds number $Re = hU/v_2$, the Weber number $We = \rho_2 U^2 h/\sigma$, and K and Ω denote the dimensionless wave number and frequency, respectively. Equation (18) can be further divided into the two following equations describing the real and imaginary parts:

$$\begin{aligned} R &: \Omega_i^2 - 2\Omega_i K_r + (K_r^2 - K_i^2) + (2\Omega_i K_r K_i - 3K_r^2 K_i + K_i^3)/Re - (K_r^2 - K_i^2)/We + \rho K_r = 0 \\ I &: -2\Omega_i K_i + 2K_r K_i + (K_r^3 - 3K_r K_i^2 - \Omega_i K_r^2 + \Omega_i K_i^2)/Re - 2K_r K_i/We + \rho K_i = 0 \end{aligned} \tag{19}$$

For given flow conditions and wave number K_r, the system of non-linear equations was solved simultaneously for the spatial growth rate K_i and wave frequency Ω_i using the Newton–Raphson method.

3. RELATIONS OF TEMPORAL AND SPATIAL INSTABILITIES

As liquid issues from a nozzle, its surface is subjected to disturbances. These include vibrations of the nozzle, gas motion surrounding the liquid surface, turbulence in the liquid, and roughness of the nozzle inner wall. For linear stability analysis, the disturbances may be described in a Fourier form:

$$\delta = \delta_0 \cdot \mathrm{e}^{\mathrm{i}kx + \omega t} \tag{20}$$

where δ_0 is the initial amplitude of the disturbance. In temporal instability analysis, the wave number ($k = k_r$) is a real number and the wave frequency ($\omega = \omega_r + i\omega_i$) is a complex number. The real part of the frequency ω_r determines the degree of wave amplification or damping, and is defined as the temporal wave growth rate.

In the past, Squire [1] analysed the linear stability of an inviscid sheet of constant thickness using the temporal method. Dombrowski and Johns [9] extended his study to a viscous film of diminishing thickness for a more realistic consideration. In their temporal analyses, a dispersion equation was derived from the equations of motion to predict the growth rate ω_r of disturbance with wave number k_r for a given flow condition. The temporal dispersion equation of Dombrowski and Johns [9] is given as

$$\rho_2 h\omega_r^2 + \mu_2 h k_r^2 \omega_r + \sigma k_r^2 - \rho_1 k_r U^2 = 0 \tag{21}$$

In order to compare with the spatial growth rates, the temporal growth rates ω_r for a spectrum of wave numbers k_r in Equation (21) were also computed in the present study.

On the other hand, it is necessary to discuss the relationship between the two growth rates. According to Gaster's study [16] for small rates of amplification, the spatial growth is related to the temporal growth by the dimensionless group velocity, $\partial\Omega_i/\partial K_r$, which is given as

$$\frac{(\Omega_r)_T}{(K_i)_S} = \frac{\partial \Omega_i}{\partial K_r} \tag{22}$$

where $(\Omega_r)_T$ and $(K_i)_S$ are the dimensionless growth rates of temporal and spatial theories respectively. In the present study, our numerical results, as shown in Figure 2, confirmed Gaster's theory [16] and the relationship between the temporal and spatial analyses of Lin and Kang [19] for liquid cylindrical jets. Figure 2 demonstrates the solutions of dimensionless wave frequency Ω_i vs wave number K_r for the case of $Re = 1000$, $\rho = 0.001$, and $We = 300$.

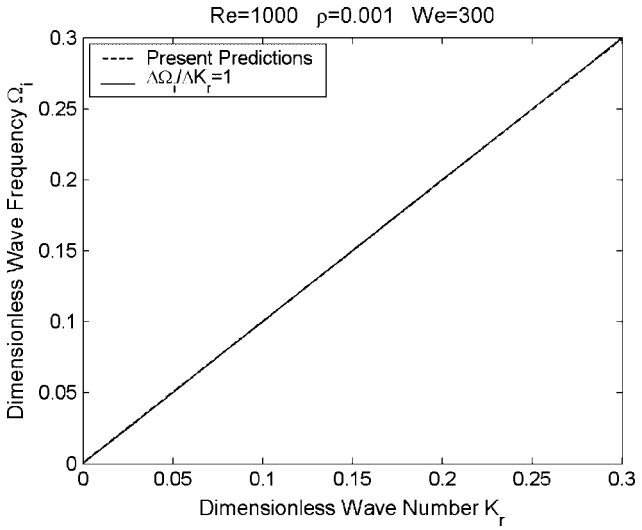

Figure 2. Dimensionless solutions of wave frequency Ω_i vs a spectrum of disturbance wave numbers K_r for a viscous liquid sheet.

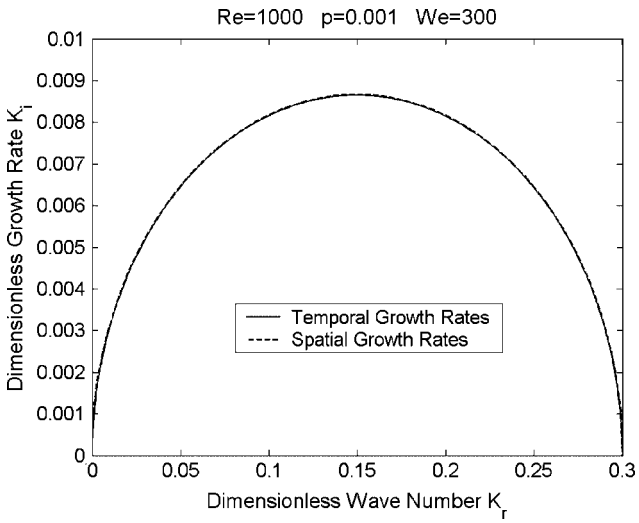

Figure 3. Comparison of spatial and temporal instability of sinuous disturbances for a viscous liquid sheet.

In Figure 2, it is clear that the gradient $\Delta\Omega_i/\Delta K_r$ of the present solutions is equal to one and that the dimensional relation gives:

$$\frac{\partial \Omega_i}{\partial K_r} = \frac{\partial \omega_i}{U \cdot \partial k_r} = 1 \quad \text{and} \quad \frac{\partial \omega_i}{\partial k_r} = U \tag{23}$$

As a matter of fact, the present spatial instability is based on an inertia frame, while the temporally growing disturbances of Dombrowski and Johns [9] may be viewed in a reference frame travelling at the liquid velocity U. Therefore, the group velocity $\partial\omega_i/\partial k_r$ appears to be the velocity U and is verified in Equation (23). By substituting the results of Equation (23) into Gaster's equation (22), the equal relationship of dimensionless temporal and spatial growth rates (i.e. $(\Omega_r)_\mathrm{T} = (K_i)_\mathrm{S}$ can be obtained for the case of $Re = 1000$, $\rho = 0.001$, and $We = 300$. This can also be validated by the solutions of growth rates for the same conditions, as shown in Figure 3. In Figure 3, the dimensionless spatial and temporal growth rates of liquid film instability are plotted as a function of dimensionless wave number. It can be seen that the temporal growth rates $(\Omega_r)_\mathrm{T}$ represented by a solid curve are essentially equal to the spatial results $(K_i)_\mathrm{S}$ represented by a dashed curve.

4. EFFECTS OF WEBER NUMBER

The Weber number is defined as $We = \rho_2 U^2 h/\sigma$ and represents the ratio of the inertia force to surface tension. For cylindrical liquid jets, the Weber number is an important physical parameter to identify capillary breakup regimes. In the present study of a two-dimensional liquid sheet, the Weber number also plays a critical role. Figure 4 shows dimensionless variations of spatial and temporal growth rates of a spectrum of disturbance wave

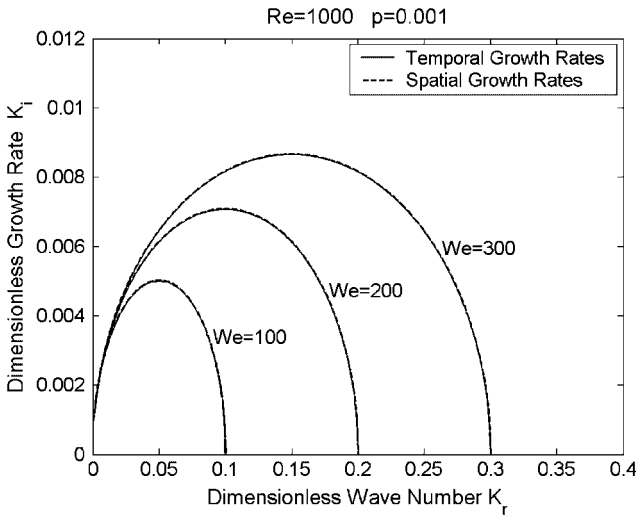

Figure 4. Comparison of spatial and temporal instability of sinuous disturbances for a viscous liquid sheet at various Weber numbers ($We = 100$, 200, and 300).

numbers for three different Weber numbers. As shown in Figure 4, when the Weber number is high, the temporal growth rates are basically the same as the spatial growth rates. It is evident that the temporal results of Dombrowski and Johns [9] agreed quite well with the present spatial solutions for these conditions of $We \geqq 100$. The temporal results, as shown in Figure 4, are similar to the theoretical studies for cylindrical jets at high Weber numbers [19, 27], which have shown a good agreement between the temporal predictions and experiments.

However, the spatial instability predicted different results from those of the temporal analysis for low-speed liquid sheets where $We < 100$. Figures 5 and 6 demonstrate the discrepancy between temporal and spatial instability as the Weber number fell below 100. This discrepancy tends to be larger as the Weber number becomes smaller. It was observed that the temporal theory of Dombrowski and Johns [9] underestimated the growth rates, especially for disturbances with long wavelengths. This explains why the temporal instability theory is unable to predict accurately at low-flow-rate conditions [28]. This result is similar to the results of low-speed cylindrical jets described by Keller *et al.* [18] and Lin and Kang [19].

According to the present analysis for a two-dimensional liquid sheet, surface tension always stabilizes the flow. However, it can be a destabilizing factor in the case of low-speed cylindrical jets [29] when the disturbance wavelength is larger than the jet circumference. Figures 4–6 show that the flow becomes more stable as surface tension increases when other parameters keep constant. The Weber number can also imply the flow rate when surface tension remains constant. The maximum growth rate tends to be higher and shifts toward the shorter wavelength range with the increase of Weber number. This indicates that, for a two-dimensional liquid film, the breakup length becomes shorter and drop size becomes smaller as the flow rate increases.

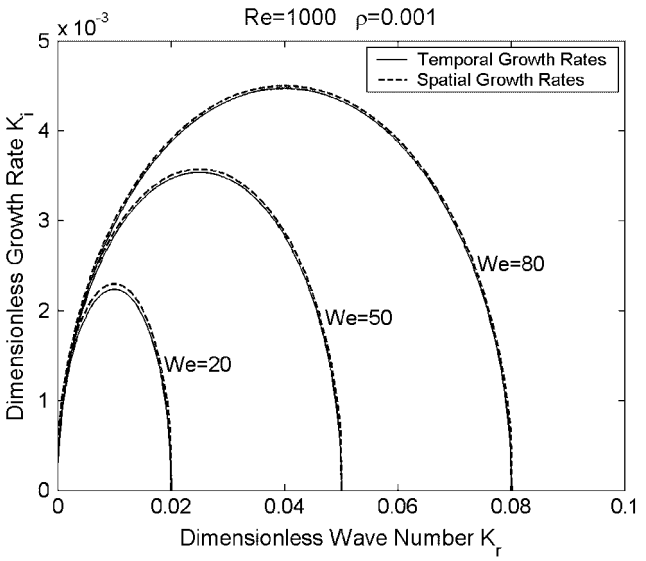

Figure 5. Comparison of spatial and temporal instability of sinuous disturbances for a viscous liquid sheet at various Weber numbers ($We = 20$, 50, and 80).

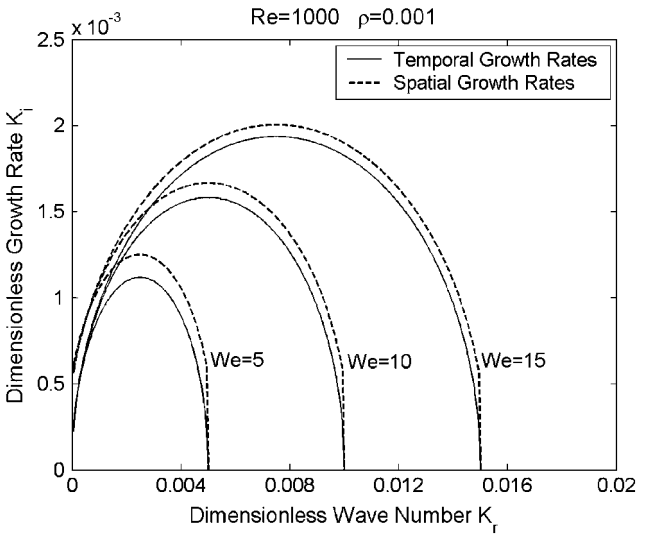

Figure 6. Comparison of spatial and temporal instability of sinuous disturbances for a viscous liquid sheet at various Weber numbers ($We = 5$, 10, and 15).

5. EFFECTS OF REYNOLDS NUMBER

As expected, the liquid's viscosity is a damping factor during the process of wave growth. As indicated in Figure 7, the maximum growth rate decreases as the Reynolds number decreases.

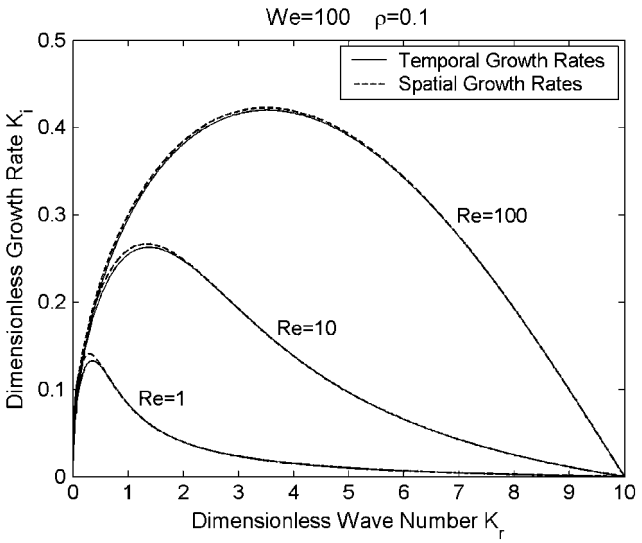

Figure 7. Comparison of spatial and temporal instability of sinuous disturbances for a viscous liquid sheet at various Reynolds numbers ($Re = 1$, 10, and 100).

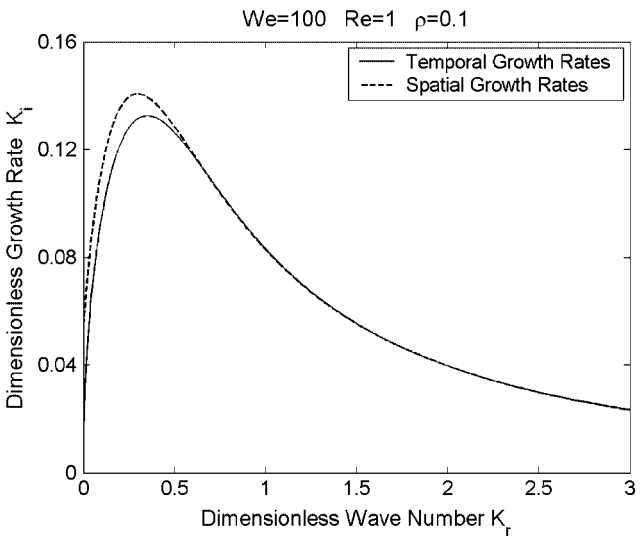

Figure 8. Close-up plots of dimensionless wave growth rate vs wave number for a viscous liquid sheet ($We = 100$, $Re = 1$, $\rho = 0.1$).

It should be noted that there is a slight deviation between the temporal and spatial results for all values of *Re*. This again indicates that the temporal theory tends to underestimate the growth rates at relatively low flow conditions. With a decrease in Reynolds number, the deviations between the two theories become larger, especially for small wave numbers. This can be observed more clearly in the close-up plots of $Re = 1$ and 10, as shown in Figures 8 and 9.

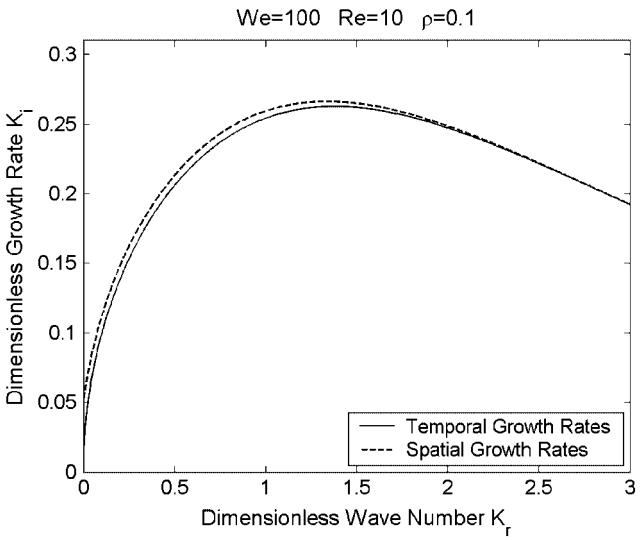

Figure 9. Close-up plots of dimensionless wave growth rate vs wave number for a viscous liquid sheet ($We = 100$, $Re = 10$, $\rho = 0.1$).

It is interesting that, in Figure 7, the growth rates for the larger wave numbers decrease significantly as the Reynolds number decreases. In other words, the decreasing rate of the shorter-wave growth rates is higher than that of the longer-wave growth rates when the flow viscosity is increased. Waves of very small length are difficult to be excited because of viscous dissipation. Waves of very long length have relatively low growth rates and are slow to develop due to inertial effects. Between the extremely short and long wavelengths, there exists a growth peak, which corresponds to the most unstable wave. In Figure 8, the case of $Re = 1$ clearly demonstrates these phenomena. In addition, the maximum growth rate appears in the smaller wave number range when the flow becomes more viscous, as shown in Figures 7–9. This implies that, for a very viscous liquid sheet, only large drops and ligaments can be formed during the breakup process.

6. EFFECTS OF DENSITY RATIO

The relation between the growth rate and the wave number is shown in Figure 10 for the cases of gas/liquid density ratio $\rho = 0.001$, 0.005, and 0.01. If the case of $\rho = 0.001$ represents water in air at room temperature and one atmosphere, then the approximate pressures of the ambience for $\rho = 0.005$ and 0.01 are 5 and 10 atm, respectively, at room temperature. Similar to the effects of the Weber number, the growth rates are increased and the maximum growth rate shifts to a smaller wavelength range as the gas/liquid density ratio is increased. Accordingly, the liquid film becomes more unstable and atomization will be finer in the higher-pressure environment due to the inertia effect of air on the disturbance waves. In Figure 10, the discrepancy between the spatial and temporal solutions is not significant.

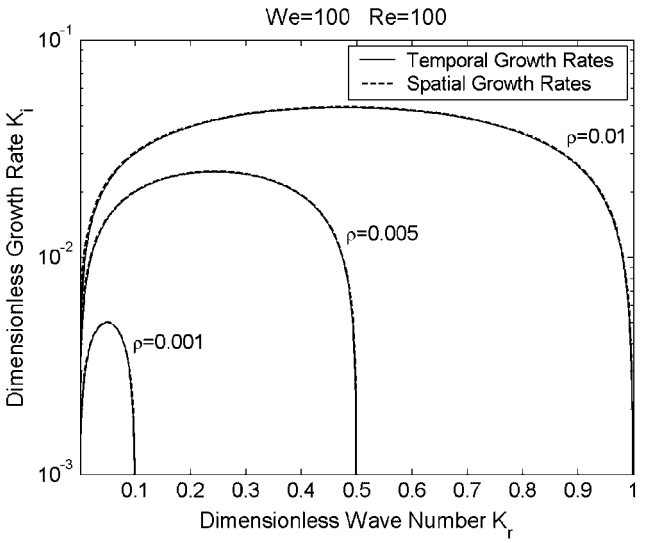

Figure 10. Dimensionless wave growth rate vs wave number for a viscous liquid sheet at various gas/liquid density ratios ($\rho = 0.001$, 0.005, and 0.01).

7. CRITICAL WAVE NUMBER AND WAVELENGTH

It should be noted that there exists a critical wave number (i.e. cut-off wave number), which distinguishes the stable and unstable wave disturbances for each case. Disturbances that have wave numbers larger than the critical wave number will not grow (i.e. $K_i = 0$). Thus, the dimensionless critical wave number, K_c, can be obtained analytically through Equation (19) and expressed as follows:

$$K_c = \rho We \tag{24}$$

This can also be verified graphically from the results of Figures 4–10. In dimensional terms, Equation (24) can be expressed as

$$\lambda_c = \frac{2\pi h}{\rho \cdot We} = \frac{2\pi\sigma}{\rho_1 U^2} \tag{25}$$

where λ_c is the critical wavelength. It means that disturbances with wavelengths shorter than the critical wavelength are stable; otherwise, they are unstable and their growth rates are positive. It is interesting that, according to Equation (25), the impact of the capillary length $\sigma/\rho_1 U^2$ on the disturbance wave instability for a two-dimensional liquid sheet is exactly the same as its role in cylindrical jets [25].

Based on Equation (25), the gas/liquid density ratio and the Weber number determine the wavelength range of unstable disturbances and the shortest wavelength in this range. For the cases of $\rho = 0.001$, 0.005, and 0.01 in Figure 10, the shortest unstable wavelengths are 6.28, 1.256, and 0.628 mm, respectively, if half of the liquid sheet thickness $h = 0.1$ mm is assumed.

Similarly, for the cases of various Weber numbers in Figures 4–6, the unstable wave range and the shortest wavelength can also be obtained.

8. CONCLUSIONS

The major conclusions of the present study are as follows:

1. The Weber number is the most important variable affecting the discrepancy between spatial and temporal instability.
2. For a two-dimensional liquid sheet, the temporal instability analysis provides reasonably accurate solutions of growth rates for conditions with Weber numbers greater than 100.
3. The temporal theory generally underestimates growth rates. The discrepancy between the results of temporal and spatial theory increases as the Weber number decreases.
4. The theories of both temporal and spatial instability predict that flow disturbances become more unstable and the disturbance with a maximum growth rate shifts toward the shorter wavelength range as either the Weber number or the gas/liquid density ratio increases. This indicates that a two-dimensional liquid film has a shorter breakup length and produces finer drops at higher flow rate or pressure conditions.
5. For a two-dimensional sheet, liquid viscosity and surface tension always play a role of stabilizing the flow disturbances. For a very viscous liquid sheet, only large drops and ligaments are formed during sheet breakup.
6. A critical wave number can be identified from the Weber number and gas/liquid density ratio to distinguish the stable and unstable flow disturbance regimes for a two-dimensional liquid sheet.

REFERENCES

1. Squire HB. Investigation of the instability of a moving liquid film. *British Journal of Applied Physics* 1953; **4**:167–169.
2. Lamb H. *Hydrodynamics* (6th edn). Dover: New York, NY, 1945.
3. Taylor GI. The dynamics of thin sheets of fluid. *Proceedings of the Royal Society of London* 1959; **253**: 289–321.
4. Taylor GI. Formation of thin flat sheets of water. *Proceedings of the Royal Society of London* 1960; **A259**:1–17.
5. York JL, Stubbs HE, Tek MR. The mechanism of disintegration of liquid sheets. *Transactions of the ASME* 1953; **75**:1279–1286.
6. Haggerty WW, Shea JF. A study of the stability of plane fluid sheets. *Journal of Applied Mechanics* 1955; **22**:509–515.
7. Fraser RP, Eisenklam P, Dombrowski N, Hasson D. Drop formation form rapidly moving liquid sheets. *AIChE Journal* 1962; **8**:672–680.
8. Dombrowski N, Hooper PC. The effect of ambient density on drop formation in sprays. *Chemical Engineering Science* 1962; **17**:291–305.
9. Dombrowski N, Johns WR. The aerodynamic instability and disintegration of viscous liquid sheets. *Chemical Engineering Science* 1963; **18**:203–214.
10. Crapper GC, Dombrowski N, Jepson WP, Pyott GAD. A note on the growth of Kelvin–Helmholtz waves on thin liquid sheets. *Journal of Fluid Mechanics* 1973; **57**:671–672.
11. Lefebvre AH. *Gas Turbine Combustion*. Hemisphere: New York, NY, 1983.
12. Li X, Tankin RS. On the temporal instability of a two-dimensional viscous liquid sheet. *Journal of Fluid Mechanics* 1991; **226**:425–443.
13. Rangel RH, Sirignano WA. Nonlinear growth of Kelvin–Helmholtz instability: Effect of surface tension and density ratio. *Physics of Fluids* 1988; **31**:1845–1855.
14. Rangel RH, Sirignano WA. The linear and nonlinear shear instability of a fluid sheet. *Physics of Fluids A* 1991; **3**:2392–2400.

15. Mehring C, Sirignano WA. Nonlinear capillary wave distortion and disintegration of thin planar liquid sheets. *Journal of Fluid Mechanics* 1999; **388**:69–113.
16. Gaster M. A note on the relation between temporally-increasing and spatially-increasing disturbances in hydrodynamic stability. *Journal of Fluid Mechanics* 1962; **14**:222–224.
17. Gaster M. Growth of disturbances in both space and time. *Physics of Fluids* 1968; **11**:723–727.
18. Keller JB, Rubinow SI, Tu YO. Spatial instability of a jet. *Physics of Fluids* 1973; **16**:2052–2055.
19. Lin SP, Kang DJ. Atomization of a liquid jet. *Physics of Fluids* 1987; **30**:2000–2006.
20. Lin SP. Stability of a viscous liquid curtain. *Journal of Fluid Mechanics* 1981; **104**:111–118.
21. Lin SP, Roberts G. Waves in a viscous liquid curtain. *Journal of Fluid Mechanics* 1981; **112**:443–458.
22. Creighton B, Lin SP. Mechanism of atomization of liquid sheets. *Atomization and Sprays* 1991; **1**:187–197.
23. Li X. Spatial instability of plane liquid sheets. *Chemical Engineering Science* 1993; **48**:2973–2981.
24. Ibrahim EA. Spatial instability of a viscous liquid sheet. *Journal of Propulsion and Power* 1995; **11**:146–152.
25. Levich VG. *Physicochemical Hydrodynamics*. Prentice-Hall: Englewood Cliffs, NJ, 1962.
26. De Luca L, Costa M. Instability of a spatially developing liquid sheet. *Journal of Fluid Mechanics* 1997; **331**:127–144.
27. Chuech SG, Przekwas AJ, Singhal AK. Numerical modeling for primary atomization of liquid jets. *AIAA Journal of Propulsion and Power* 1991; **7**:879–886.
28. Mao CP, Chuech SG, Przekwas AJ. An analysis of pressure swirl and pure airblast atomization. *Journal of Atomization and Sprays* 1991; **1**:215–235.
29. Rayleigh L. On the instability of jets. *Proceedings of London Mathematical Society* 1879; **10**:4–13.

